

HEAT TRANSFER ANALYSIS OF BIO-PRINTED TISSUE MIMICKING  
MATERIAL MIXED WITH SILVER NANOPARTICLES

Jedeshkeran Chandrasegaran, B.Sc.

Thesis Prepared for the Degree of  
MASTER OF SCIENCE

UNIVERSITY OF NORTH TEXAS

August 2022

APPROVED:

Tae-Youl Choi, Major Professor  
Xiaohua Li, Committee Member  
Weihuan Zhao, Committee Member  
Herman Shen, Chair of the Department of  
Mechanical Engineering  
Shengli Fu, Interim Dean of the College of  
Engineering  
Victor Prybutok, Dean of the Toulouse  
Graduate School

Chandrasegaran, Jedeshkeran. *Heat Transfer Analysis of Bio-Printed Tissue Mimicking Material Mixed with Silver Nanoparticles*. Master of Science (Mechanical and Energy Engineering), August 2022, 44 pp., 4 tables, 21 figures, 1 appendix, 27 numbered references.

Novel tissue mimicking materials have been developed for cancer treatment research. In the present research work, the tissue mimicking material is printed using 3D bioprinting technology. The nanoparticles are homogeneously mixed with tissue mimicking materials to enhance the heating capacity. The thermal conductivity of tissue mimicking materials is measured using a micropipette thermal sensor (MTS). Further, the optimal value is identified based on optimization technique and incorporated into a theoretical model to predict the surface temperature of microsphere. The heat conduction governing equation with Lambert law is numerically solved using COMSOL Multiphysics software. To validate the present simulation results, the experiments are conducted using a continuous laser system.

Copyright 2022

by

Jedeshkeran Chandrasegaran

## ACKNOWLEDGMENTS

There aren't enough words or sentiments to sufficiently express my sincere gratitude to everyone that stood by me, resiliently, to support me throughout this journey towards completing my thesis successfully.

First and foremost, I am greatly in debt to Dr. Tae- Youl Choi – my mentor and persistent advisor, for his continued support and valuable guidance during every stage of my research work. I am grateful and deeply appreciative of the enthusiasm he provided and the confidence he bestowed upon me. I couldn't have completed the research work efficiently, without his constant gestures of encouragement, and valuable insight. I conclude my research, deeply inspired by his work dynamic, sincerity, and knowledge. It was a privilege to have been mentored by him. Thank you.

I would also like to take this moment to extend my gratitude towards Dr. Sreekar Marpu – Research Assistant Professor, Department of Chemistry for offering me his expertise in chemistry, and assistance in helping me further my understanding of the chemistry behind the tissue-mimicking material.

My heartfelt thanks will also be extended to Bisola Adeyemi – Prospective Ph.D. student, Department of chemistry for her valuable time, and her swiftness to help in creating tissue-mimicking material mixed with nanoparticles.

Dr. Hyeonu Heo- Graduate Program in Acoustics at Penn State University, for his commitment and essential advice regarding bioprinting. I am profoundly thankful.

Furthermore, I am immensely thankful to National Science Foundation for awarding the funds for my research (Award number 1906553).

Lastly, I want to take a moment to express how truly grateful I am to every single person that came together to support me – directly or indirectly – throughout this strenuous but rewarding journey of completing my thesis.

## TABLE OF CONTENTS

	Page
ACKNOWLEDGMENTS.....	iii
LIST OF TABLES AND FIGURES .....	vii
LIST OF ABBREVIATIONS.....	ix
CHAPTER 1. INTRODUCTION.....	1
1.1 Objectives.....	2
1.2 Organization of the Thesis.....	3
CHAPTER 2. LITERATURE REVIEW.....	5
2.1 Heat Conduction Process .....	5
2.2 Steady-State Methods .....	6
2.3 Thermocouple Based Method.....	6
2.4 Cancer Tissue Structure .....	8
2.5 Laser Heating of Tissue Mimicking Materials (TMM) .....	9
2.6 The Beer-Lambert Law and Laser Heating.....	11
2.7 Absorption Coefficient.....	12
2.8 Scope of the Thesis .....	12
2.9 Research Questions .....	13
2.10 Summary .....	13
CHAPTER 3. MATERIALS AND METHODOLOGY .....	14
3.1 Introduction .....	14
3.2 Tissue-Mimicking Structure.....	14
3.3 TMM Mixed Homogeneously with Ag Nanoparticles.....	15
3.4 3D Bioprinter Details.....	16
3.5 Fabrication of Microspheroids using 3D Bioprinter .....	17
3.6 Characterization of Microspheroids .....	18
3.7 Simulation Results .....	19
3.8 Summary .....	20
CHAPTER 4. MEASUREMENT OF DENSITY, ABSORPTION COEFFICIENT, AND THERMAL CONDUCTIVITY .....	21

4.1	Introduction .....	21
4.2	Measurement of the TMM Density .....	21
4.3	Measurement of the Absorption Coefficient.....	22
4.4	Absorbance Measurement.....	22
	4.4.1 UV/VIS Analysis .....	23
4.5	Fabrication of Micropipette Thermal Sensor (MTS) .....	24
4.6	Calculating Thermal Conductivity .....	25
4.7	Numerical Simulation.....	26
4.8	Optimization Analysis.....	27
4.9	Summary .....	27
CHAPTER 5. THE THEORETICAL MODELING OF LASER HEATING OF TISSUE MIMICKING MATERIALS (TMM) .....		28
5.1	Introduction .....	28
5.2	Theoretical Modeling.....	28
5.3	Numerical Simulation Results .....	29
5.4	Experimental Research.....	30
5.5	Results and Discussion.....	32
5.6	Summary .....	32
CHAPTER 6. CONCLUSION AND FUTURE SCOPE.....		33
6.1	Summary .....	33
6.2	Future Scope .....	33
APPENDIX: SUPPLEMENTAL MATERIAL.....		35
REFERENCES.....		42

## LIST OF TABLES AND FIGURES

Page

### Tables

Table 3-1: Technical Specification of BIO .....	16
Table 4-1: Material Properties of TMM .....	21
Table 5-1: Laser and Material Parameters .....	28
Table 5-3: Comparison of Simulation and Experimental Results .....	32

### Figures

Figure 2-1: Schematic showing the Seebeck. ....	7
Figure 2-2: Schematic of thermocouple circuit. ....	8
Figure 2-3: Size and shape of normal and cancer cells (Shashni et al., 2018).....	8
Figure 2-4: Spheroid cancer culture configuration (Velliou et al., 2020).....	9
Figure 2-5: Schematic representation of light material interaction (COMSOL Inc). ....	12
Figure 3-1: COMSOL model images of tissue structures. (a) Normal cell outside, cancer cells inside; (b) Cancer cell outside, normal cells inside; (c) Random distribution among cancer cells and normal cells. ....	15
Figure 3-2: Photography of 3D bioprinter. ....	17
Figure 3-3: Photography of nozzles installed on a bioprinter.....	17
Figure 3-4: Image of micro spheroids obtained using laser optical microscope. (a) Micro spheroids with 420 microns diameter; (b) Micro spheroids with 280 microns diameter. ....	18
Figure 3-5: Contour images of simulation results for different tissue mimicking structures. (a) Normal cell outside, cancer cells inside; (b) Cancer cell outside, normal cells inside; (c) Random distribution among cancer cells and normal cells. ....	19
Figure 4-1: Absorption coefficient vs wavelength for Experiment 1.....	23
Figure 4-2: Absorption coefficient vs wavelength for Experiment 2.....	24
Figure 4-3: Experimental set of thermal conductivity measurement system (Shrestha et al., 2018). ....	26



Figure 4-4: 2D axisymmetric model for sensor and fluid in COMSOL and the temperature field obtained from the simulation. (a) Geometrical model used in COMSOL; (b) 3D surface plot of the sensor.....	26
Figure 4-5: Result for Experiment 1.....	27
Figure 5-1: Contour plots of temperature distribution on microsphere. (a) 3D contour plot; (b) 2D contour plot.....	29
Figure 5-2: Predicted temperature distribution from numerical simulation for Sample 1. ....	29
Figure 5-3: Contour plots of simulation results for Sample 2. (a) 3D contour plots; (b) 2D contour plots.....	30
Figure 5-4: Predicted temperature distribution from numerical simulation for Sample 2. ....	30
Figure 5-5: (a) Experimental setup; (b) closed view. ....	31
Figure 5-6: Microscopic images of microspheres during temperature measurement. (a) Sample 1; (b) Sample 2; (c) microscopic images of laser irradiated 3D bio printed microsphere .....	31

## LIST OF ABBREVIATIONS

S	Seebeck coefficient [ $\mu\text{V}/^\circ\text{C}$ ]
k	Thermal conductivity [ $\text{W}/\text{m}^\circ\text{C}$ ]
$\dot{Q}$	Heat flow [W]
A	Surface area perpendicular to heat flow [ $\text{m}^2$ ]
T	Temperature [ $^\circ\text{C}$ ]
x	Thickness/characteristic length[m]
r	Radius [m]
$\alpha$	Absorption coefficient (1/m)
h	convective heat transfer coefficient [ $\text{W}/\text{m}^2\text{K}$ ]
$T_s$	Surface temperature of sample [K]
$\rho$	Density ( $\text{Kg}/\text{m}^3$ )

## CHAPTER 1

### INTRODUCTION

Cancer is the major cause of mortality worldwide, accounting for over 10 million fatalities in 2020, or roughly one in every six deaths [1]. Despite significant advancements in cancer therapy, the high incidence of recurrence, tendency to metastasis, and development of drug resistance make cancer a serious worldwide health concern. Cancer researchers can use in vitro tumor models to replicate the Vivo tumor microenvironment, in addition to animal models, to find novel treatment methods [2]. Tissue mimicking materials (TMMs) have been employed in clinical simulations and biological research for a long time. They are usually kept within a phantom, which is a replica of the human body or a bodily portion [3]. Many researchers have investigated the use of three-dimensional (3D) printing and 3D bioprinting technologies to produce functioning medical phantoms for diverse purposes, thanks to the rapid improvement of these additive manufacturing techniques. The uses of 3D printing and 3D bioprinting technologies for the construction of functioning medical phantoms and bio-structures are discussed in this study [4].

Despite the publication of thousands of in vitro 3D cancer models since the 1990s [6, 7], and reports that 90% of Glioblastoma (GBM) cases arise de novo from glial cells [8], none to date have focused on distinguishing the various stages of those GBM which develop by multi-step tumorigenesis from glial primary human astrocytes. In this context, a human in vitro co-culture model that mimics key aspects of the 3D intracranial environment is required to offer context and quality control for our real-time assessment Micropipette Thermal Sensor (MTS) tool, as well as to facilitate its translation into in vivo animal and clinical models.

Several researchers have reported the numerical simulations on laser heating of tissue mimicking materials. Shrestha et al., (2018; 2020) have reported the transient heat diffusion model with a laser point heat source for predicting the temperature in cancer cells. They also proposed the optimization technique for identifying the thermal conductivity of materials.

In the actual laser heating process, the amount of heat energy is transferred to irradiated material depending on the absorptivity. The tissue mimicking material properties play a significant role in the laser heating process.

In this thesis, the fabrication of a novel 3D spheroid material is presented using tissue mimicking materials with a mix of nanoparticles. The micropipette thermal sensors were fabricated such that different tip sizes were produced with varying coating conditions during physical vapor deposition (PVD hereafter). The thermal sensor was calibrated with the help of a water bath chamber at a constant temperature. The material properties like thermal conductivity, absorption coefficient, and density are determined based on experimental tests. Further, optimization techniques are used to identify the optimal material properties.

The numerical simulations are carried out to predict the laser-heated surface temperature of tissues mimicking materials using finite elements based on COMSOL Multiphysics software. The predicted temperature values are compared with measured values and discussed in the present research work.

## 1.1 Objectives

The main objective of the research work is to develop a novel 3D bioprinting tissue-mimicking materials (TMM) mixed with silver nanoparticles and use it to irradiate with a

laser. The numerical simulations are carried out to investigate the thermal response of laser irradiated cancer cells.

- To develop three different cell structure with a combination of cancer and normal cells.
- To 3D bio print micro spheroids by using tissue-mimicking materials (TMM) with homogeneously mix of silver nanoparticles.
- To fabricate the micropipette thermal sensor (MTS) for measure the thermal conductivity and temperature rise of the microsphere under laser irradiation.
- To determine the material properties of TMM based on the measurement and analytical approach.
- To develop the numerical simulations for predicting the temperature rise on the microsphere under laser irradiation.
- To validate the predicted temperature values from simulation results with measured values.

## 1.2 Organization of the Thesis

Chapter 2 presents the results of the literature research. This chapter describes the modeling of laser ablation processes based on heat transfer equations. Also presented the plasmonic photothermal therapy and different tissue structure homogeneously mixed with nanoparticles. The tissue-mimicking material properties are presented.

Chapter 3 deals with the methods and materials used in the experiments. It discusses the process for the fabrication of 3D spheroid materials and tissue structure modeling.

Chapter 4 discusses the measurement of absorption coefficient, thermal conductivity, and density of the material.

Chapter 5 presents the theoretical modeling of laser heating of tissue-mimicking materials (TMM) and compared with the experimental model

Chapter 6 concludes the thesis with a summary and provides guidelines for possible future extensions of this work.

## CHAPTER 2

### LITERATURE REVIEW

This chapter briefly discusses the results of the literature research. The measurement techniques of thermal conductivity for materials and thin film are discussed. The sensors developed are thermocouples made of nickel and Bismuth and were calibrated individually as each sensor differs in tip size even though the PVD coating condition was the same for one batch of sensors. A detailed review of the laser heating on tissue-mimicking materials is presented and discussed. The literature review is extended to the effect of nanoparticles in laser heating of cancer cells.

#### 2.1 Heat Conduction Process

The laser heating process has been solved using the heat conduction equation which is represented by conventional Fourier's law. In the heat conduction process, the energy is transported through a solid medium under the influence of a temperature difference. The principle of heat conduction is stated by Fourier's law according to which the heat transfer by conduction per unit area (heat flux) in a particular direction is proportional to the negative local temperature gradient in that direction (Mills, 1995). The proportionality constant in this law is known as thermal conductivity and is denoted by the symbol  $k$ . For one-dimensional heat conduction with temperature varying in the  $x$ -*direction* only, heat flow is obtained by the equation,

$$\dot{Q} = -kA \frac{dT}{dx} \quad (2.1)$$

where:  $\dot{Q}$  = heat flow [W]

$k$  = thermal conductivity [W/m°C]

$A$  = surface area perpendicular to heat flow [m<sup>2</sup>]

$\frac{dT}{dx}$  = temperature gradient along x-direction [°C/m]

In cylindrical coordinates, with temperature varying in radial direction only, the equation for heat flow is written as

$$\dot{Q} = -kA \frac{dT}{dr} \quad (2.2)$$

where  $\frac{dT}{dr}$  = temperature gradient along r (radius) direction [°C/m]

Measuring the thermal conductivity of thin films is not standardized because each class of thin film has unique properties and obstacles that must be overcome during the experiment. However, literature reviews have shown that researchers follow, a steady-state technique to determine thermal conductivity and diffusivity.

## 2.2 Steady-State Methods

The steady-state thermal conductivity methods provide a direct assessment of the thermal conductivity of thin films and are based on the Fourier law of thermal conductivity. Most techniques use an infinitely parallel plate or cylinder as the model, and the calculation of thermal conductivity is simplified by reducing the heat transfer problem to a one-dimensional problem.

## 2.3 Thermocouple Based Method

A thermocouple is a junction between two different metals and is based on the principle that when the ends of two dissimilar metals joined together are maintained at different temperatures then the voltage is generated across the ends as shown in Fig.2.1. The Seebeck effect was named after Thomas Seebeck, who discovered it in 1821. This effect can be seen in all types of different metals. The Seebeck coefficient, or thermoelectric sensitivity of the metal, is the change in voltage as a function of



temperature.

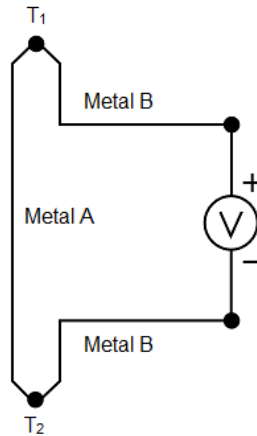


**Figure 2-1: Schematic showing the Seebeck.**

This coefficient is usually a temperature-dependent nonlinear function. For a modest change in temperature, however, the coefficient remains constant. As a result, the linear relationship between the voltage difference generated by the two metals and the accompanying temperature gradient is:

$$\Delta V_{AB} = S_{AB} \Delta T \quad (2.3)$$

where:  $\Delta V_{AB}$  = Seebeck voltage [micro Volts]

$S_{AB}$  = Seebeck coefficient [ $\mu\text{V}/^\circ\text{C}$ ]

Thermocouples are the most commonly used temperature sensors because they are inexpensive and come in a variety of sizes that can measure a wide range of temperatures. The schematic representation of a typical thermocouple circuit is shown in Fig.2.2. A conductor subjected to a thermal gradient generates Seebeck voltage, according to the Seebeck effect.

To measure this voltage, a voltmeter must be connected, which requires connecting another conductor, namely the voltmeter's lead wires. This extra lead wire will form an extra junction and generate its Seebeck voltage, which will be in opposition to the

original voltage. The magnitude of the effect is determined by the Seebeck coefficient of the various metals used.

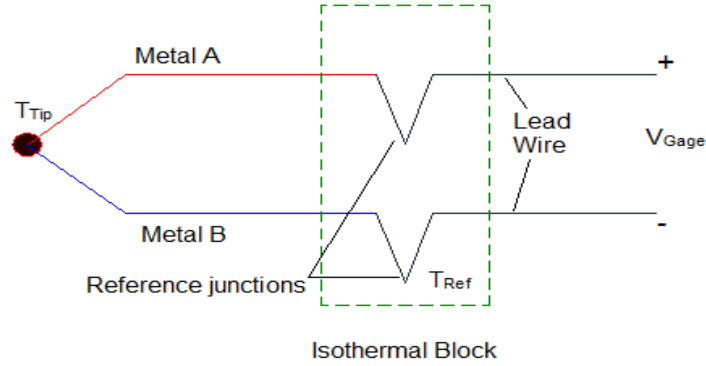


**Figure 2-2: Schematic of thermocouple circuit.**

## 2.4 Cancer Tissue Structure

The tumors in the body have a much different surface area, shape, and cellular composition than cultured cells, so data from cancer treatment trials will differ from the reaction of a real tumor to the drugs. It's important to develop a novel approach for mimicking the actual tissue structure of cancer cells. Shashni et al., (2018) have reported the size and shape of normal and cancer cells based on the Particle Size Analyzer. The different sizes of cancer cells' dimension ranges are shown in Fig.2.3.

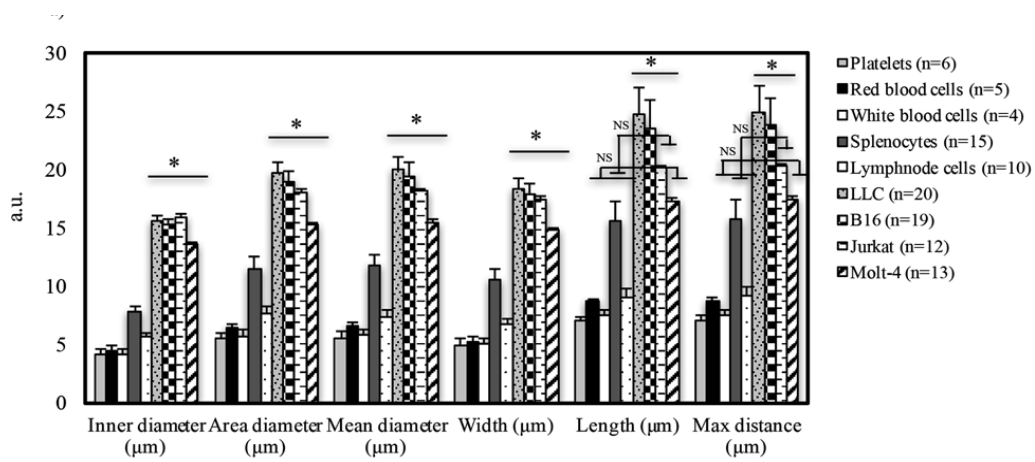


**Figure 2-3: Size and shape of normal and cancer cells (Shashni et al., 2018).**

Ficarella et al., (2019) have reported the size of a cancer cell as 15  $\mu\text{m}$ , and a normal cell size of 10  $\mu\text{m}$ . Velliou et al., (2020) have developed 3D cancer models based on biomaterials and opened up new routes to comprehend and fight dismal tumors. The schematic representation of spheroid cancer culture cell configuration is shown in Fig.2.4.

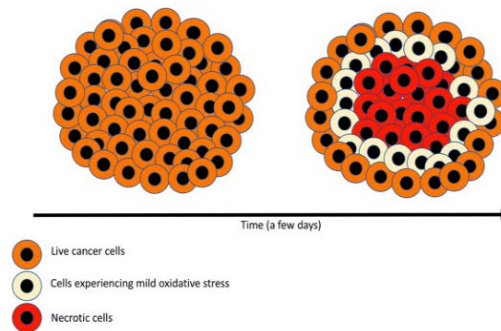


**Figure 2-4: Spheroid cancer culture configuration (Velliou et al., 2020).**

These models can be used to investigate phenomena such as tumor growth at an early stage, malignant cell migration, and cell-cell interactions. Finally, advanced 3D models are more ethically sustainable, reliable, and reproducible on a large scale at a low cost than animal models, which are more complex, costly, and difficult to replicate. As a result, advanced 3D models are a promising approach for personalized medicine as well as the development of novel targeted and functional therapies. As a result, biomaterial-based 3D cancer models are predicted to open up new avenues for understanding and combating dreadful malignancies like the Pancreatic ductal adenocarcinoma (PDAC).

## 2.5 Laser Heating of Tissue Mimicking Materials (TMM)

Several researchers have used the laser heating process to kill cancer cells by localized heating in the literature. The computation approach has been developed to investigate the laser heating of cancer cells. Fuentes et al., (2009) have developed a

computational model for bioheat transfer into living tissue in real-time, laser treatments of prostate cancer monitored by magnetic resonance thermal imaging.

The effect of the addition of nanoparticles to irradiated tissue on the thermal sink behavior of LBVs has been studied in the literature (Paul et al., 2016). Negussie et al., (2021) have reported the tissue-mimicking thermochromic (TMTC) phantom material that changes color permanently when heated can be used to examine volumetric thermal heating patterns as well as maximum temperatures for a low cost. The creation, formulation, and use of a TMTC phantom material with thermochromic ink that permanently changes color from white to magenta when heated to temperatures above 60°C were discussed. This phantom material can be used for thermal therapy quality assurance and device evaluation, and the phantom formulation can be adjusted to suit different thermal therapies (e.g., laser, RF, HITU, and MW) or tissue attributes.

Bin Xie et al 2012 have presented thermal maps obtained via magnetic resonance imaging characterizing laser heating of a phantom tissue containing a multiwalled carbon nanotube inclusion. Also, the modeling methodology validated in this work will assist in optimizing the application of nanoparticles in thermal tumor heating by allowing the precise application of ablative heat temperatures with minimal spillover to surrounding structures. Soltani et al., (2020) reported that the microwave heating of tumors can be improved by the injection of magnetic nanoparticles (MNPs). The effectiveness of this technique, evaluated by the dimensions of the heating zone, is related to the MNPs' concentration and the MWA input power and frequency. Singh, S., & Melnik(2020) reported that computational modeling was a powerful tool for studying the effect of electromagnetic interactions within the biological tissues and predicting the treatment

outcomes during thermal ablative therapies. Sokolovskaya et al.,(2021) have analyzed the feasibility of employing SiNPs produced by the laser heating of silicon nanowire arrays in water and ethanol as agents for laser tumor hyperthermia, and numerically simulated the effects of heating a millimeter-sized nodal basal-cell carcinoma with embedded nanoparticles by continuous-wave laser radiation at 633 nm. Ashikbayeva, et al., (2019) have reported that nanomaterials can generate and specifically enhance the heating capacity in the tumor region due to optical and magnetic properties. The mentioned unique properties of nanomaterials allow inducing the heat and destroying the cancerous cells.

Fernandes et al., (2021) have reported that the absorption properties of nanoparticles play a significant role in the localized heating of cancer cells without significantly damaging nearby healthy tissues.

## 2.6 The Beer-Lambert Law and Laser Heating

The absorption of the laser energy has been described by the Beer-Lambert law. When light strikes materials, part of the energy is absorbed by the material. It is assumed that the light is a single wavelength, collimated (like from a laser), and suffers very little refraction, reflection, or scattering inside the material itself, and may use the Beer-Lambert formula to describe the light intensity. For light intensity, this rule may be stated in differential form as:

$$dI/dz = \alpha(T)I \tag{2.4}$$

where  $z$  is the beam direction coordinate and  $\alpha$  is the material's temperature-dependent absorption coefficient. The governing partial differential equation can be solved for predicting the temperature distribution in spatial and time coordinates.

$$\rho c p \left( \frac{dT}{dt} \right) - \nabla k(\nabla T) = Q = \alpha(T)I \quad (2.5)$$

where the heat source term, Q, equals the absorbed light.

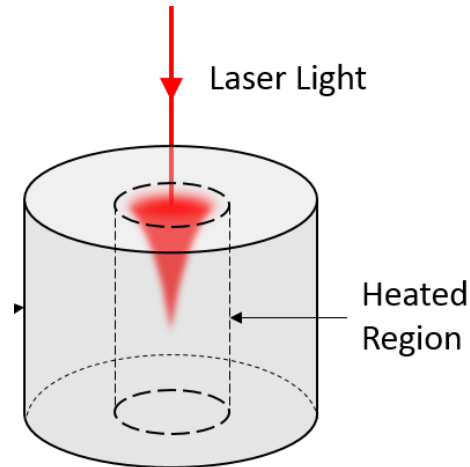


**Figure 2-5: Schematic representation of light material interaction (COMSOL Inc).**

## 2.7 Absorption Coefficient

The absorption coefficient of laser-heated material plays an important role in the laser heating process. Therefore, the absorption coefficient of tissue-mimicking materials is obtained from UV/VIS spectrophotometer and discussed in the next Chapter.

## 2.8 Scope of the Thesis

The bioprinted 3D microspheroids have been widely used for cancer treatment research. Numerous research has been carried out on cancer treatment based on theoretical models. The present research work is useful in the selection of optimal material properties for tissue-mimicking materials. The bioprinted 3D microspheroids have been widely used for cancer treatment research. The tissue-mimicking materials mixed with nanoparticles will have a significant role in bio tissue engineering applications.

## 2.9 Research Questions

The novel tissue-mimicking materials with a mix of nanoparticles has been used to develop the theoretical model of cancer treatment in the literature. However, the material properties such as thermal conductivity and absorption coefficient of tissue-mimicking materials are not available in the literature. Realistic geometric models are required to mimic the actual tissue structure of cancer cells.

The heat transfer analysis of tissue-mimicking materials needs to be developed to investigate the thermal response of micro spheroids. The proposed simulation approach needs to be validated with experimental results.

## 2.10 Summary

A detailed literature review on the measurement of thermal conductivity has been presented and discussed. The modeling of laser heating of tissue-mimicking material is presented and discussed in this chapter. Also, the influence of nanoparticles in the bio heating process has been studied. The material and methodology of the present research work are discussed in the next chapter.

## CHAPTER 3

### MATERIALS AND METHODOLOGY

#### 3.1 Introduction

In the present chapter, the modeling of tissue structure is presented using COMSOL Multiphysics software. The materials used in the present work are explained with chemical composition. The details of the 3D bioprinter and nozzles are discussed. The fabrication and characterization of 3D bioprinted microspheroids are presented and discussed in this chapter. The numerical simulations are conducted to predict temperature rise in a tissue-mimicking structure in the laser heating process. The simulation results are presented and discussed in this chapter.

#### 3.2 Tissue-Mimicking Structure

The different distribution of tissue-mimicking structure was already reported in the literature (Velliou et al.2020) as discussed in Chapter 2. In the present research work, three different tissue-mimicking structures are modeled in COMSOL Multiphysics software. The geometric models are built using circle primitives of different sizes as shown in Fig.3.1. The tissue-mimicking structures are listed below:

- 1) Normal cells outside cancer cells inside
- 2) Cancer cells outside normal cells inside
- 3) Random distribution

The random distribution of circles is created with the help of a JavaScript program, which is used as an Application Program Interface (API) in COMSOL Multiphysics software. Further, the booleans operation is carried out for interlinking cells. The Sample Javascript program is can be found in the appendix.



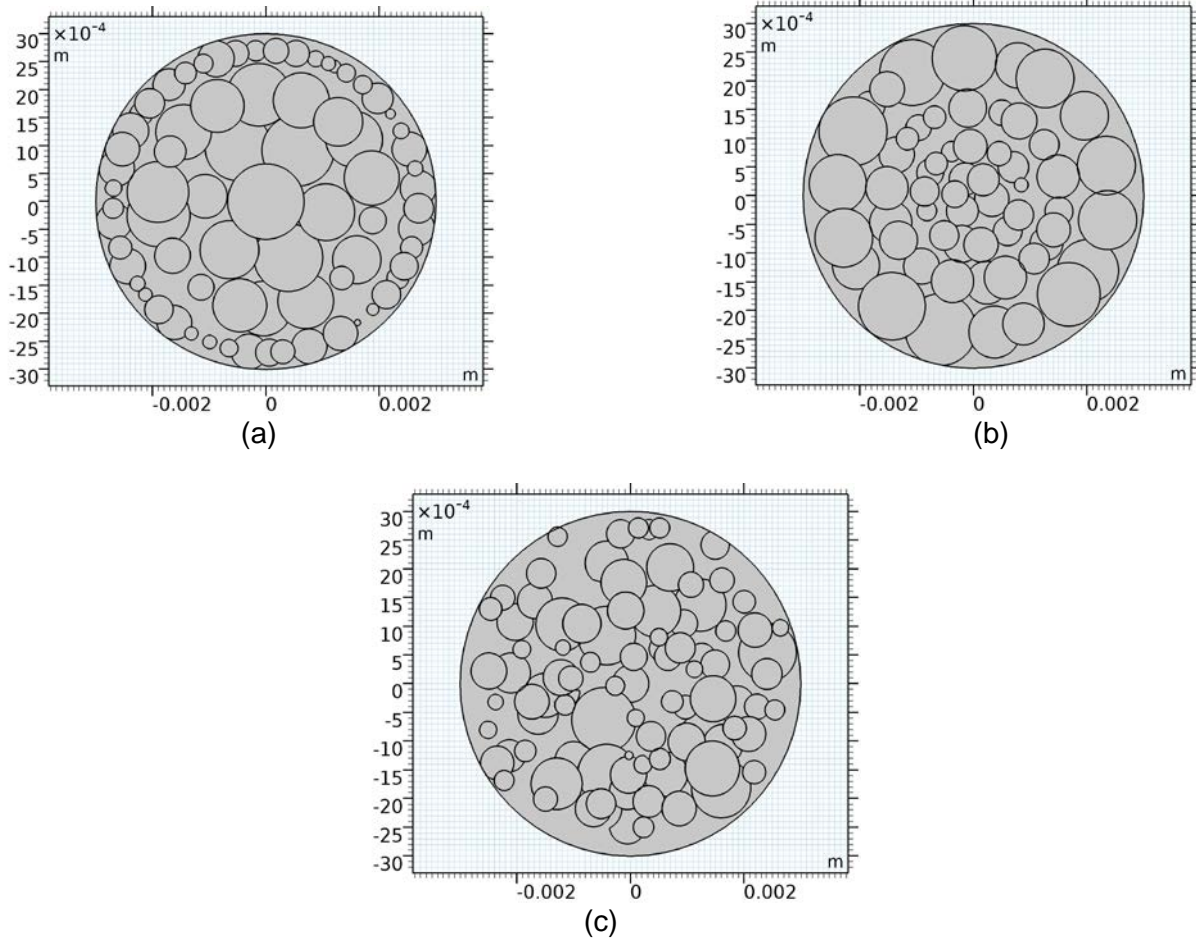


**Figure 3-1: COMSOL model images of tissue structures.** [about:blank](#) (a) Normal cell outside, cancer cells inside; (b) Cancer cell outside, normal cells inside; (c) Random distribution among cancer cells and normal cells.

### 3.3 TMM Mixed Homogeneously with Ag Nanoparticles

Alginate gel 5% was dissolved in water in a 5-gram clear glass vial and mixed at room temperature for 20 to 30 minutes with a stir bar on a magnetic stirrer. The gel solution was then added to a solution of silver nitrate salt and agitated for another 10 to 15 minutes. The resulting solution was irradiated while being stirred constantly to ensure homogeneity. Irradiation with an American Ultraviolet Spectrum 100 arc lamp converted silver salt to silver nanoparticles at three-minute interval for each of three cycles, until the UV spectra of the sample did not change. Using a Schlenk line, the dilute silver

nanoparticle gel was concentrated to 90 percent w/V concentration. TMM can be combined with another hydrogel to produce an ionically cross-linkable composite. Calcium chloride (CaCl<sub>2</sub>) was used in this study to crosslink, which is useful for toughening the microspheroids.

### 3.4 3D Bioprinter Details

In the present research work, the 3D bioprinter is used to print microspheroids (Make Cellink, USA, Model: BIO X). The built-in features along with the new BIO X software managed through the large touchscreen display minimize the learning curve and ensure accurate results (Cellink, USA). Technical specifications of BIO X printer details are given In Table 3-1.

**Table 3-1: Technical Specification of BIO**

<b>Specification/Parameter</b>	<b>Values/ Data</b>
Weight, kg	18
Build Volume, mm	130 x 90 x 70 mm
Build surface compatibility	Multi-well plates, Petri dishes, glass slides
Resolution XY, μm	1
Layer Resolution, μm	1
Pressure range (internal pump), kPa	0-200
Pressure range (external air supply), kPa	0-700
No. of printhead slots	3
Photocuring sources (built-in), nm	365, 405, 485, 520
Printbed temperature range, °C	4-65
Printhead temperature range, °C	4-250 (printhead specific)
Filter class, chamber air-flow	HEPA 14
UV-sterilization	UV-C (275nm), 20mW output
Calibration Options	Manual and Automatic
Supported file formats, software	.gcode, .stl

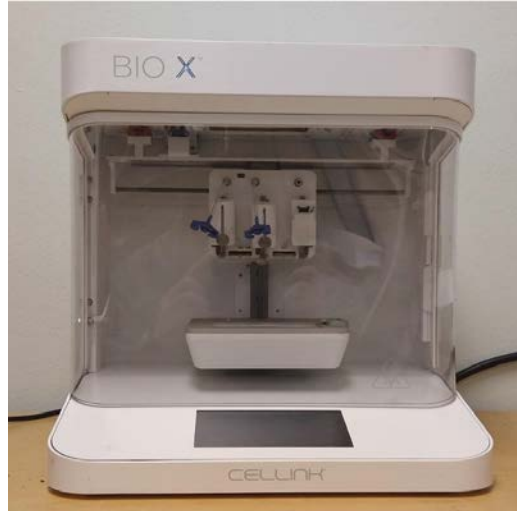


**Figure 3-2: Photography of 3D bioprinter.**

### 3.5 Fabrication of Microspheroids using 3D Bioprinter

In the present research work, the main objective is to print microspheroids close to the Vivo cancer cell diameter range. The microspheroids are printed with sizes of 280 - 420  $\mu\text{m}$  due to the limitations of the equipment. However, the size of the cells is ranging from 10-15  $\mu\text{m}$  in living tissue cells.

In the present work, two different sets of sterile micron precision conical nozzles are used that have an inner diameter of 50 and 100  $\mu\text{m}$  respectively. These nozzles were installed on the 3D bioprinter as shown in Fig. 3.3.

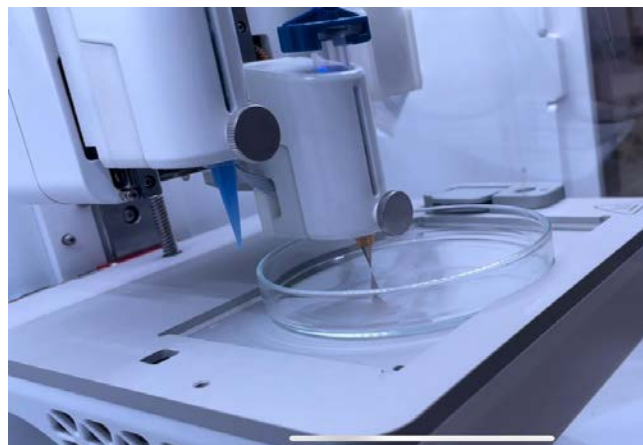


**Figure 3-3: Photography of nozzles installed on a bioprinter.**

Protocols for 3D bioprinter:

- 1) Start the bioprinter and insert the petri dish into which the cell will be printed.
- 2) Insert a 3ml syringe containing the appropriate sample into one of the three pressurized sides.
- 3) Select Droplet printing and enter the number of rows and columns to print, as well as the distance between each droplet.
- 4) The appropriate pressure (50kPa) and extrusion time (1.5s) are selected.
- 5) Calibrate the printer before printing.

To reduce the formation of spheroids on the tip of the nozzle rather than the petri dish, ensure that the tip of the sensor almost touches the petri dish during calibration.

- 6) Number of cells is printed with a selection option.
- 7) After printing the microspheroids crosslink the spheroids with  $\text{CaCl}_2$  solution.
- 8) The solidification time was set based on the required size of microspheroids.
- 9) The microspheroids are filtered from the  $\text{CaCl}_2$  solution, and then stored in the refrigerator.

### 3.6 Characterization of Microspheroids

The 3D bioprinted microspheroids are characterized using a laser optical microscope (Make: Keyence, Japan). The scanned images are shown in Fig. 3.4, it is observed that the minimum size of the sphere is about 280  $\mu\text{m}$ , whereas the maximum size of the sphere is 420  $\mu\text{m}$ .



**Figure 3-4: Image of micro spheroids obtained using laser optical microscope. (a) Micro spheroids with 420 microns diameter; (b) Micro spheroids with 280 microns diameter.**

### 3.7 Simulation Results

In the present work, preliminary simulations are carried out to investigate the laser heating of tissue structure. The laser heat conduction model with the Lambert law is used to generate localized heating on a tissue-mimicking structure (discussed in the previous chapter). The heat conduction model governing equation is solved using the finite element approach in COMSOL Multiphysics software. The predicted contour plots of laser heated tissue structures are shown in Fig 3.5.

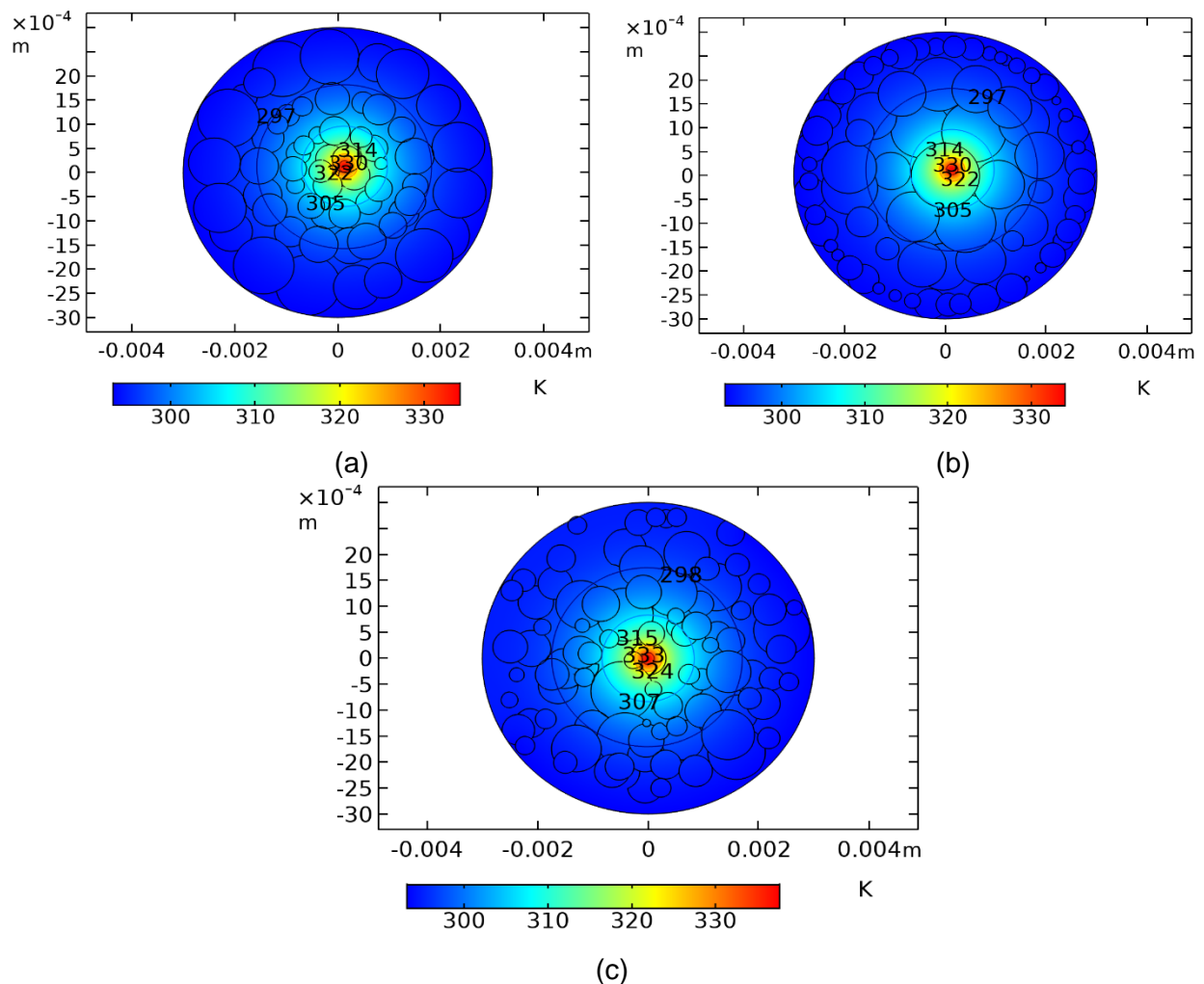


**Figure 3-5: Contour images of simulation results for different tissue mimicking structures. (a) Normal cell outside, cancer cells inside; (b) Cancer cell outside, normal cells inside; (c) Random distribution among cancer cells and normal cells.**

From the above results it is observed that the maximum temperature rises about 324 K at the central position of tissue structure. Also, the contour plots show that temperature value decreases from central position. The proposed simulation approach is extended to simulate a single spheroid and discussed in Chapter 5.

### 3.8 Summary

The geometrical modeling of different tissue structures is presented using COMSOL Multiphysics software. The 3D bioprinting of microspheroids is demonstrated and discussed in the present chapter. The simulation shows a temperature rise in tissue structure. The tissue mimicking materials properties measurement techniques are presented and discussed in Chapter 4.

## CHAPTER 4

### MEASUREMENT OF DENSITY, ABSORPTION COEFFICIENT, AND THERMAL CONDUCTIVITY

#### 4.1 Introduction

The first part of this chapter presents the density measurement of TMM. Later thermal conductivity value of the different concentrations of TMM mixed homogeneously with Ag nanoparticles will be presented. Finally, the absorption coefficient will be discussed for the above-mentioned samples.

#### 4.2 Measurement of the TMM Density

For this experiment, a simple mathematical calculation is conducted to estimate the density of the TMM. To conduct this mathematical calculation, the mass and the volume data are obtained. The gel is dispensed into the syringe to the correct volume, then transferred into an empty vial that was placed on top of the weighing scale to determine its mass. The mass and volume data are incorporated in the equation (4.1) and the density value is estimated for 4 samples. The estimated density values are given in Table 4.1. The mean and standard deviation are obtained as 0.9986 (g/ml) and 0.102.

$$Density = \frac{Mass(g)}{Volume (ml)} \quad (4.1)$$

**Table 4-1: Material Properties of TMM**

Mass (G)	Volume (ml)	Density (G/ml)
1.2223	1.1	1.1111
0.936	1.0	0.936
0.8902	1.0	0.8902
1.057	1.0	1.057

### 4.3 Measurement of the Absorption Coefficient

The absorption coefficient value of TMM material wasn't provided by the manufacturer so the below mathematical equation was derived from the Lambert law to calculate it.

$$I = I_0 e^{(-\alpha t)} \quad (4.2)$$

where

$I = \text{Transmitted Energy}$  ;  $I_0 = \text{Incident Energy}$  ;

$\alpha = \text{Absorption Coefficient}$  ;  $t = \text{thickness of the material}$

By simplifying Equation (4.2) to Equation (4.3)

$$\frac{I}{I_0} = e^{(-\alpha t)} \quad (4.3)$$

Taking logarithms on both sides of Eqn. (4.3)

$$\log \left( \frac{I}{I_0} \right) = (-\alpha t) \log (e) \quad (4.4)$$

$$-\log \left( \frac{I}{I_0} \right) = (\alpha t) \log (e) \quad (4.5)$$

Substitute  $\log (e) = 0.434$

$$\alpha = \frac{-\log \left( \frac{I}{I_0} \right)}{0.434t} \quad (4.6)$$

$\left( \frac{I}{I_0} \right) < 0$ , therefore substitute  $(-\log \left( \frac{I}{I_0} \right)) = A$ , where  $A = \text{Absorbance}$

$$\alpha = 2.304 \frac{A}{t} \quad (4.7)$$

The above equation derived shows that Absorbance needs to be measured to calculate the absorption coefficient.

### 4.4 Absorbance Measurement

The absorbance of material can be measured using a UV/VIS spectrometer. The



details of the UV/VIS analysis are discussed in the next section.

#### 4.4.1 UV/VIS Analysis

PerkinElmer Lambda 900 UV/VIS/NIR spectrophotometer was used to obtain UV/VIS data. The analysis was conducted on different concentrations of the 5% alginate gel using a 1mm cuvette. Pure 5% alginate gel was run in between transparent glass slides due to the viscosity of the gel and the thickness was determined using vernier calipers. The analysis was done on the gel containing silver nanoparticles using a 1cm cuvette.

##### 4.4.1.1 Experiment 1

12 %TMM and 88% water homogeneously mixed with 0.3% of 0.03mM  $\text{AgNO}_3$ . The results of absorbance vs wavelength have been converted to the equation above to absorption coefficient, so Figure 4-1 illustrates the absorption coefficient vs wavelength.

In Experiment 1, MGL-III-532 Green laser is used and has a wavelength of  $532 \pm 1$  nm. In the above graph for the green laser, the approximate absorption coefficient is around 610.

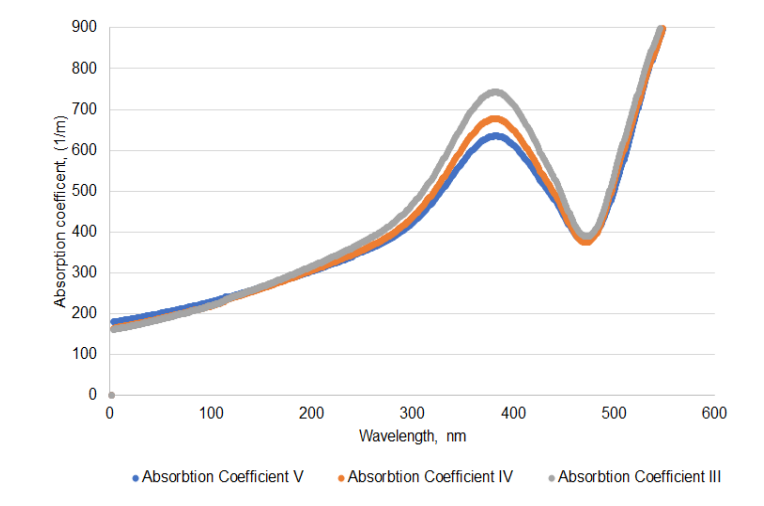


**Figure 4-1: Absorption coefficient vs wavelength for Experiment 1.**

#### 4.4.1.2 Experiment 2

10% TMM gel 90% water homogeneously mixed with 0.3% of 0.03mM AgNO<sub>3</sub>. In Experiment 2, MGL-III-532 Green laser is used and has a wavelength of 532±1 nm. In the above graph for the green laser, the approximate absorption coefficient is around 600.

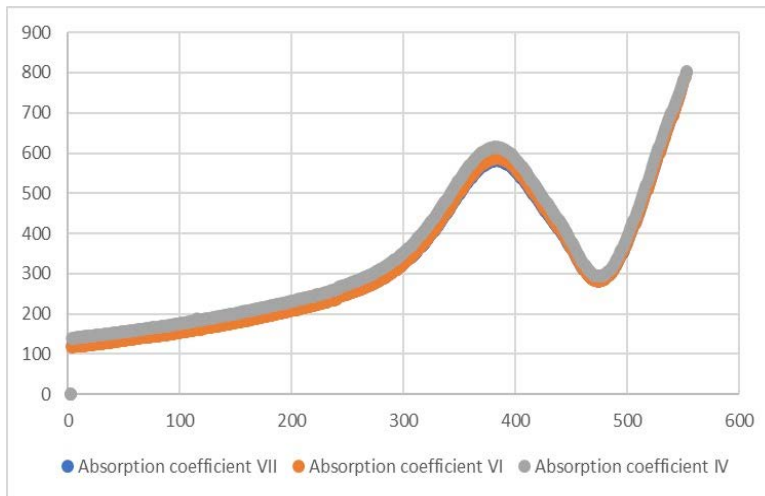


**Figure 4-2: Absorption coefficient vs wavelength for Experiment 2.**

#### 4.5 Fabrication of Micropipette Thermal Sensor (MTS)

The first step in MTS fabrication is to pull the borosilicate glass to a tip with a diameter of 1-2 microns. The shutter instrument (P-97) was used to heat borosilicate glass and pull in-between to form a tip with a diameter of 1-2 microns. After being pulled, the pipette was filled with bismuth (Bi) alloy using an injection molding process and localized heating of the material. This was achieved through the use of a small heating chamber and the mechanical pushing of a servo actuator. The heating chamber was kept at 270°C, which melts the metal inside the chamber, and the liquid metal was pushed to the tip under the microscope's observation. Excess metal from the pipette tip must be ground away to create the junction. This is necessary to ensure a good connection between the inner and outer metals.

The tip was sharpened and smoothed using the Microforge-Grinding Center MFG-5APT, which is designed for beveling micropipettes with tip diameters between 0.1 and 50  $\mu\text{m}$ . This procedure was monitored using a 20x microscope mounted on the Microforge-Grinding Center. The pipette was then sonicated to remove any debris before being coated. Sputtering or physical vapor deposition was used to apply the coating. The vacuum in the chamber is then reduced to  $10^{-6}$  Torr. The high-energy plasma is created by pumping argon gas into the chamber. The target receives 150 watts of power, and the sputtering process takes 35 minutes. This results in a nickel coating thickness of 200-250 nm on the pipette's exterior. Copper wire is connected to the inner core of bismuth after the pipette has been coated. The MTS can then be checked for resistance to ensure there is no short in the circuit. After completion of coating tip diameter is obtained in a range of 2-4 microns.

#### 4.6 Calculating Thermal Conductivity

The novel approach is proposed to calculate the thermal conductivity of material using the laser heating process in the literature (Shrestha et al., 2018). The approach is based on laser point heating thermometry and transient heat transfer and uses a micropipette thermal sensor (MTS) with a tip diameter of 2  $\mu\text{m}$ . A laser beam is irradiated at the sensor tip, which is touching the center of the TMM microsphere.

The finite element approach in the COMSOL software is used to generate a numerical solution for a transient temperature profile for a point source. The multi-parameter fitting technique in MATLAB is used to identify the optimum parameters such as thermal conductivity and power absorbed at the sensor tip, which will fit the COMSOL simulation result with the experimental data.

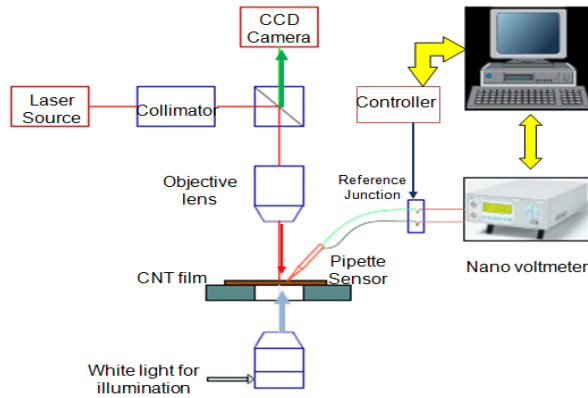


**Figure 4-3: Experimental set of thermal conductivity measurement system (Shrestha et al., 2018).**

In the present work, the MTS sensor was calibrated with known thermal conductivity of liquid and confirmed that the thermal conductivity measurement method can be used with high accuracy and estimate the thermal conductivity of the tissue-mimicking material. In this experiment, the laser is shined on the micropipette tip while the tip is touching the surface of the TMM 3D printed spheroids.

#### 4.7 Numerical Simulation

FEM analysis was carried out using a 2D axisymmetric model of the micropipette sensor surrounded by the fluid domain in the COMSOL Multiphysics software. The screenshot of the FE simulation is shown in Fig. 4.4

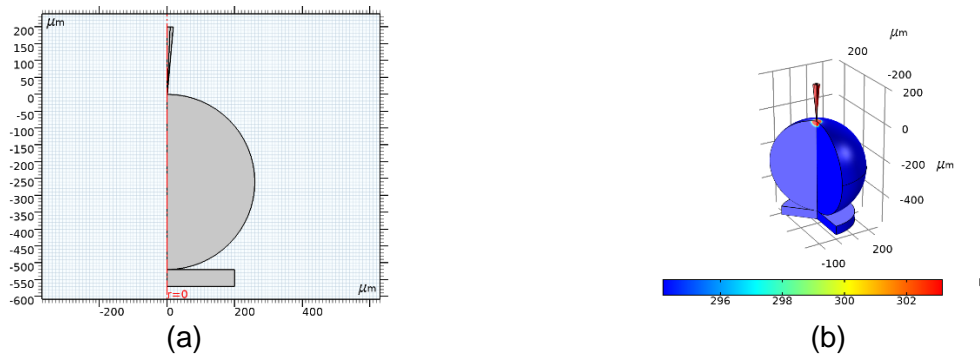


**Figure 4-4: 2D axisymmetric model for sensor and fluid in COMSOL and the temperature field obtained from the simulation. (a) Geometrical model used in COMSOL; (b) 3D surface plot of the sensor.**

#### 4.8 Optimization Analysis

The multi-parameter fitting technique is used with MATLAB software to determine the ideal values. The Nelder-Mead complex algorithm is used in the built-in algorithm "fminsearch" (Shrestha et al. 2018). A similar approach is followed to determine the optimal thermal conductivity, radius, and power in the present work. The optimization analysis screenshots are given in Figure 4-5.

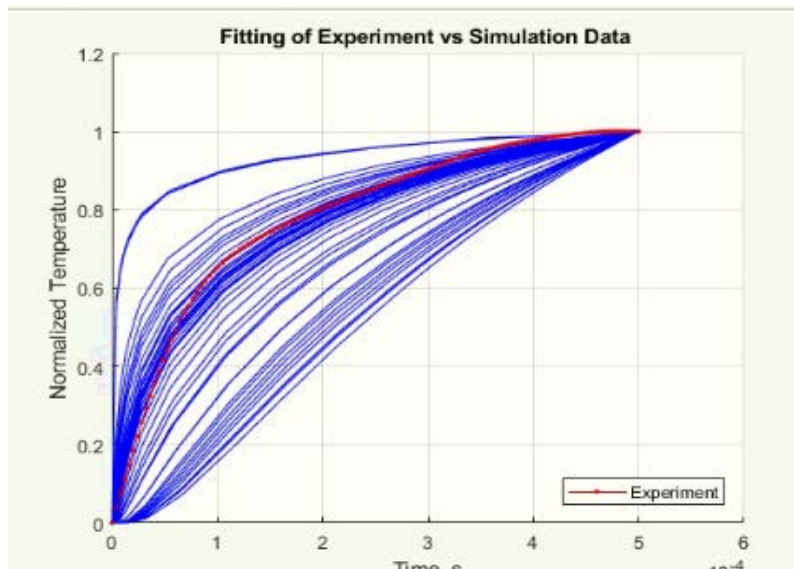


**Figure 4-5: Result for Experiment 1.**

#### 4.9 Summary

The material properties such as thermal conductivity and absorption coefficients of tissue mimicking materials are measured. The absorption coefficient is calculated as 600 and 610  $\text{m}^{-1}$  for Experiments 1 and 2 respectively.

The measured data is analyzed with optimization techniques to identify the optimal values. Numerical simulations are carried out to mimic the laser heating process. The optimal thermal conductivity of TMM obtained are 0.709 and 0.699  $\text{Wm}^{-1}\text{K}^{-1}$  for Experiments 1 and 2 respectively.

## CHAPTER 5

### THE THEORETICAL MODELING OF LASER HEATING OF TISSUE MIMICKING MATERIALS (TMM)

#### 5.1 Introduction

In the present work, the theoretical model is presented to predict temperature rise on tissue mimicking materials. The material properties identified from optimization analysis are incorporated in the present model. The predicted temperature rise on tissue mimicking material is validated with measured temperature value. The temperature measurement techniques are presented and discussed in this Chapter.

#### 5.2 Theoretical Modeling

In the present work, numerical simulations are carried out to predict the temperature rise on tissue mimicking materials using COMSOL Multiphysics software. The heat conduction module is used to solve the laser heating problem. The Lambert law is used to penetrate laser energy on tissue mimicking material. In the present work, the simulations are conducted to predict the surface temperature of laser irradiation on the spheroid. The two samples are selected with different concentrations of Ag nanoparticles (as discussed in Chapter 4). The laser parameters and material properties are given in

Table 5.1

**Table 5-1: Laser and Material Parameters**

Parameter	Variable	Value	Units
Laser			
laser beam spot radius	$r_0$	135	$\mu\text{m}$
Power	Q	0.1	W
Material			
Thermal conductivity	$k$	0.709	$\text{Wm}^{-1}\text{K}^{-1}$

Parameter	Variable	Value	Value	Units
density	$\rho$	998.6	998.6	$\text{kg m}^{-3}$
heat capacity	$C_p$	4375	4375	$\text{J kg}^{-1}\text{K}^{-1}$
Absorption coefficient	$\alpha$	610	600	$\text{m}^{-1}$

### 5.3 Numerical Simulation Results

The simulation results are presented for Samples 1 and 2 and shown in Figs. 5.1 to 5.4.

From simulation results, it was observed that the maximum temperature rise surface of the 3D printed spheroid was 295.9K with a concentration of 12%TMM and 88% water homogeneously mixed with 0.3% of 0.03mM  $\text{AgNO}_3$ . The change in temperature is 2.75 K as shown in Fig. 5.2. The maximum temperature is obtained from simulation results using global plot option in COMSOL Multiphysics software.

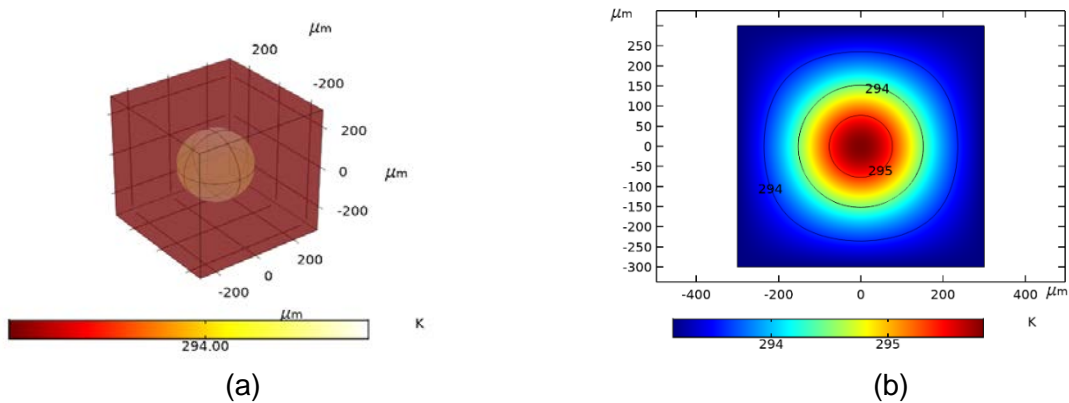


**Figure 5-1: Contour plots of temperature distribution on microsphere. (a) 3D contour plot; (b) 2D contour plot.**

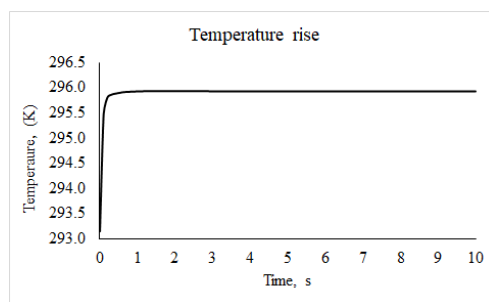


**Figure 5-2: Predicted temperature distribution from numerical simulation for Sample 1.**

Simulation results for Sample 2 having a concentration of 10% TMM gel 90% water homogeneously mixed with 0.3% of 0.03mM AgNO<sub>3</sub> are shown in Fig.5.3. It is observed that the maximum temperature rise on the surface of the 3D printed sphere 294.6K. The change in temperature is 1.45K.

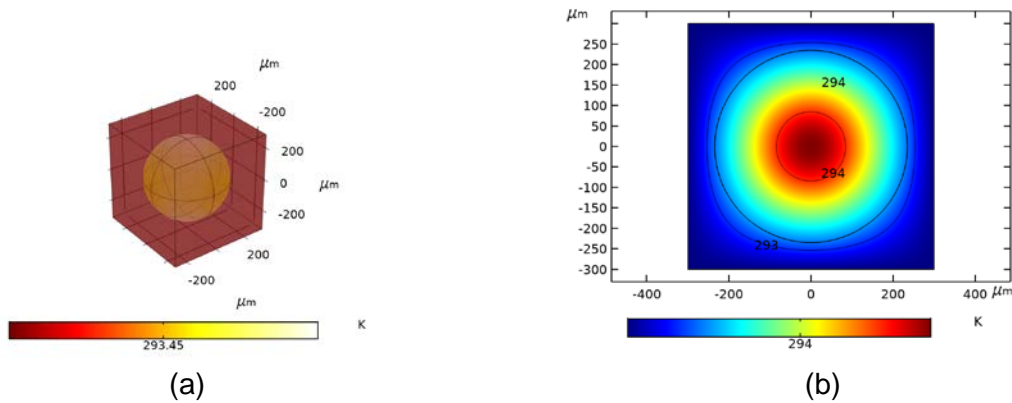


**Figure 5-3: Contour plots of simulation results for Sample 2. (a) 3D contour plots; (b) 2D contour plots.**

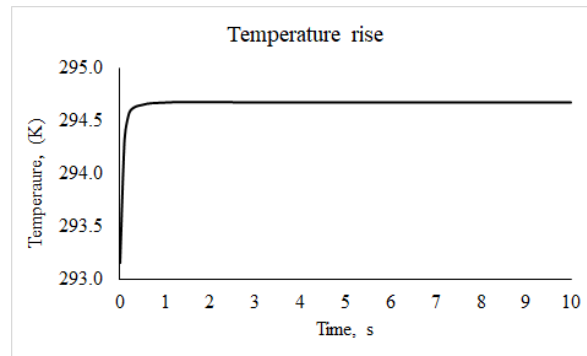
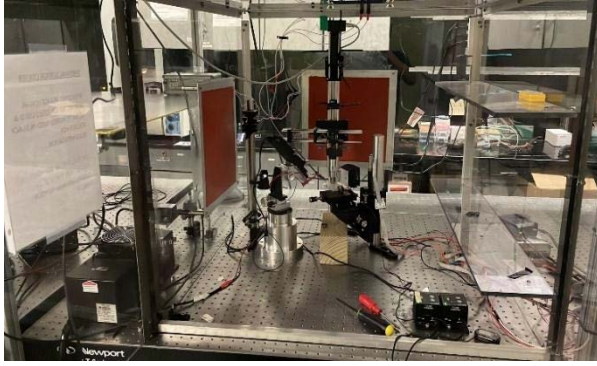


**Figure 5-4: Predicted temperature distribution from numerical simulation for Sample 2.**

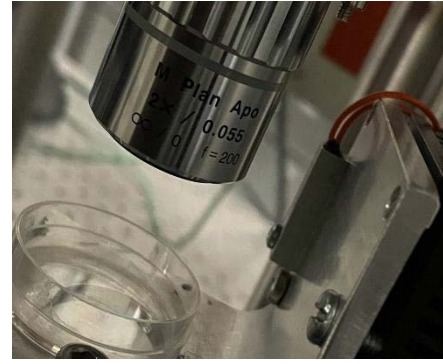
#### 5.4 Experimental Research

In the present research work, the experiments are carried out using a high-power laser system (Model: MGL-III-532 Green). The laser is focused on the center of the spheroid and the rise of temperature was measured on the edge using a micropipette thermal sensor (MTS). Steady laser light is irradiated while measuring the surface of the spheroid. Different positions are traced to get a better reading. See Fig. 5-5.



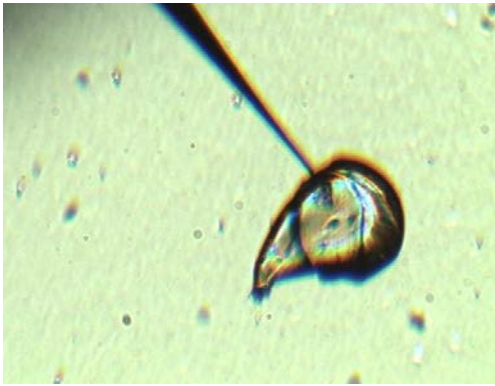


(a)



(b)

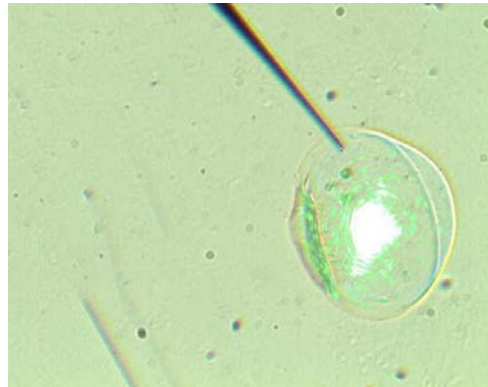
**Figure 5-5: (a) Experimental setup; (b) closed view.**



(a)



(b)



(c)

**Figure 5-6: Microscopic images of microspheres during temperature measurement. (a) Sample 1; (b) Sample 2; (c) microscopic images of laser irradiated 3D bio printed microsphere**

The voltage was recorded using an oscilloscope before laser irradiation in the middle of the microsphere. As the laser continuously irradiated on the microsphere,

voltage readings are taken. The average value is estimated from voltage data. The equation of seeback is used to convert the temperature in postprocessing. The experimental value is estimated at 2.0668 K. Similarly, the experimental value is estimated at 1.235 K for Sample 2.

## 5.5 Results and Discussion

The comparison predicted and measured temperature values are given in Table 5.3. From these results, it is observed that the deviation between measured and predicted values are 23% and 15% respectively for Sample 1 and 2. This mainly due to contamination of samples with harsh environments and do not have clean room facilities. Also, silver nanoparticles not homogeneously mixed with TMM.

**Table 5-2: Comparison of Simulation and Experimental Results**

	Measured Temperature (K)	Predicted Temperature (K)	Deviation (%)
Sample 1	2.067	2.750	23
Sample 2	1.235	1.450	15

## 5.6 Summary

The numerical simulations are carried out to investigate the thermal response on microsphere of tissue mimicking materials under laser heating. The predicted surface temperature is compared with the measured temperature value. It is observed that the maximum deviation of 23 % and 15% for Samples 1 and 2 respectively.

## CHAPTER 6

### CONCLUSION AND FUTURE SCOPE

#### 6.1 Summary

In the present research work, novel method of tissue mimicking cell structure has been discussed and experiments were conducted on the single cell level microspheroids.

Homogeneously mixed Tissue-Mimicking structure with nanoparticles was achieved.

Optimization and absorbance tests were conducted to add to the simulation model.

Two different concentrations of samples are prepared namely:

- Sample 1: 12 %TMM and 88% water homogeneously mixed with 0.3% of 0.03mM AgNO<sub>3</sub>.
- Sample 2: 10% TMM gel 90% water homogeneously mixed with 0.3% of 0.03mM AgNO<sub>3</sub>.

Laser beam was continuously shined on the microsphere which caused a change in temperature which was later justified by the simulation single microsphere model.

The thermal conductivity of the microsphere is obtained as 0.709 and 0.699 W m<sup>-1</sup>K<sup>-1</sup> for Samples 1 and 2 respectively.

The absorption coefficients of the microsphere is estimated as 610 and 600m<sup>-1</sup> for Samples 1 and 2 respectively.

The measured surface temperature rise on the edge of the microsphere is about 2.0668 and 1.235 K for Samples 1 and 2 respectively.

#### 6.2 Future Scope

The proposed simulation approach can be extended to 3D tissue structure, which will be realistic to cancer cell structure. The high-power laser can be used to heat the

microsphere. The Heat Capacity of the TMM can be measured and plugged into the COMSOL model for better simulation results. Conduct multiple experiments to prove the Ag ions have been completely dissolved to form Ag particles.

APPENDIX  
SUPPLEMENTAL MATERIAL

## Random distribution of microspheres using COMSOL (API) JavaScript program

```
1. for (int k = 26; k < 35;)
2. {
3.   for (int ang = 45; ang < 360;)
4.   {
5.     model.component("comp2").geom("geom2").run("rot25");
6.     model.component("comp2").geom("geom2").create("rot"+k, "Rotate");
7.     with(model.component("comp2").geom("geom2").feature("rot"+k));
8.       set("keep", true);
9.     endwhile();
10.    with(model.component("comp2").geom("geom2").feature("rot"+k).selection("input
    "));
11.    set("rot25");
12.    endwhile();
13.    with(model.component("comp2").geom("geom2").feature("rot"+k));
14.      set("rot", ang);
15.      set("selresult", true);
16.    endwhile();
17.    model.component("comp2").geom("geom2").runPre("fin");
18.    ang = ang+45;
19.    k++;
20.  }
21.}
```

## Matlab program for optimization

1. %%%%%%%%% %This is the code for determining the Temperature at any point (x,y,z) due to the
2. % point source at origin (0 0 0)
3. %%%%%%%%%%END OF PROGRAM%%%%%%%%%
4. %% Start with the default options
5. options = optimset;
6. %% Enter the Initial Guess for parameters
7. cond\_fluid =0.60; % Thermal conductivity of fluid/sample (W/mK)
8. r\_int = 6; % Point at which Temperature is extracted
9. p\_laser = 0.1; % Laser power in Watts
10. x0 = [cond\_fluid r\_int p\_laser]; % Setting up matrix for initial guess
11. % Set the tolerance value for the function value and the parameters for fitting
12. TolFun\_Data = 1e-3;
13. TolX\_Data = 1e-3;
14. %% Modify options setting to control the display while simulation is running
15. options = optimset(options,'Display', 'final');
16. options = optimset(options,'PlotFcns', { @optimplotfval });
17. options = optimset(options,'TolFun', TolFun\_Data);
18. options = optimset(options,'TolX', TolX\_Data);
19. %%Start the optimization of parameters using the in-built fminsearch code
20. [X,fval,exitflag, output] = fminsearch(@Everror\_RS1, x0, options);
21. % everror\_rs is MATLAB function file that is used to calculate the difference function F
22. %and fit the experiment data with the simulation.
23. %%%%%%%%%%END OF PROGRAM%%%%%%%%%

## Matlab program for error evaluation

```
1. %%%%%%%%%% Evaluation of error (difference function) (Start)%
2. function error = Eerror_RS (~)
3. %% Define control parameters (parameters to be optimized)
4. % Start of main program uncomment line 7-9
5. % cond_fluid = position(1);           %Parameter assigned with initial guess
6. % r_int = position(2);
7. % p_laser = position(3);
8. % % Use this when testing code
9. cond_fluid = .6;           %Parameter assigned with initial guess
10.r_int = 4;
11.p_laser = 100e-6;
12.%%%%%%%%%
    %%%
13.%%Define fixed parameters for COMSOLsimulation.
14.tip_p = 0.81e-6;           %tip of the pipette in m
15.cell_a = 210e-6;           % radius of cell/sphere in m
16.step = 2e-6;               % time step for simulation in sec.
17.tp = 500e-6;               % total time for simulation in sec.
18.%%Reading temperature data from experiment and smoothing the data
19.%% Read the experiment data recorded by oscilloscope
20.data = readtable('Trial 2.xlsx','Sheet','Sheet1','Range','A2:B2503');
21.data = table2array(data);
22.
23.tempexp = data(:,2);        %temperature data from experiment
24.time = data(:,1);          %time interval from the
    experiment
25.size_data = size(tempexp);
26.M = max(size_data);
27.%% Data smoothing using smoothing-spline fitting to average out experiment
    data and
28.% reduce noise data
29.[xData, yData] = prepareCurveData(time, tempexp);
30.% Set up fit type and options.
31.ft = fitype('smoothingspline' );
32.opts = fitoptions( ft );
33.opts.SmoothingParam = 0.90;
34.opts.Normalize = 'on';
35.%Fit model to data.
36.[fitresult, ~] = fit( xData, yData, ft, opts );
```



```

37.
38. yy1 = fitresult(xData);
39. tempexpsm = yy1'; %Save smoothed Temperature to a column
    matrix
40. Tmin = tempexpsm(1);
41. Tmax = tempexpsm(M);
42. %%%%%%%%%% Normalization of temperature data after smoothing raw data
43. tempexpn= zeros(1, M); % initiating loop with zeros matrix
44. for i = 1:M
45.   tempexpn(i)= (tempexpsm(i)-Tmin)/(Tmax-Tmin);
46. end
47. %% To save computation time extract data every 'n' times interval
48. n= 10; % number of data to extract every interval
49. N=round((M-1)/n); % Number of data after extracting
50. timestep= tp/(N-1); % time interval to be used in COMSOL for simulation
51. TimeX = 0:timestep:tp;
52. TempX = zeros(1, N); % initiating loop with zeros
53. TempX(1) = tempexpn(1);
54. for i = 2:N
55.   TempX(i) = tempexpn(n*(i-1) + 1);
56. end
57. %%%%%%%%%% Loading COMSOL model and setting fixed parameters
58. model=mphload('Comsol_Cell_2.mph'); % loads COMSOL model saved with the
    %specified COMSOL file name
59. model.param.set('tip_p',strcat(num2str(1e3*tip_p),'[mm]'));
60. model.param.set('cell_a',strcat(num2str(1e3*cell_a),'[mm]'));
61. model.param.set('step',step);
62. model.param.set('tp',tp);
63. %%%%%%%%%%Setting control parameters and starting COMSOL simulation
64. model.param.set('cond_fluid',cond_fluid);
65. model.param.set('p_laser',p_laser); % This power of the laser
66. %Run the COMSOL simulation
67. model.geom('geom1').run;
68. model.mesh('mesh1').run;
69. model.sol('sol1').run;
70. %%%%%%%%%%Post processing: Fetching temperature data from
    simulation at specified point coordinate
71. point_coord = [0; -r_int];
72. t= mphinterp(model,'t','coord',point_coord); %time from simulation

```

```

73. T = mphinterp(model,'T','coord',point_coord);    %evaluation of Temperature at
    r_int
74. A= [t; T'];
75. %%%%%%%%%%%%%%%%%%%%%%%%%%%%%%%%%%%%%%%%%%%%%%%%%%%%%%%%%%
    %%%
76. %% Saving simulation data to text file
77. fid=fopen('data_sim_T.txt','wt');
78. fprintf(fid,'%6.4e %6.4f\n',A);
79. fclose(fid);
80.
81. %Reading simulation temperature data
82. fin2 = fopen('data_sim_T.txt','r');
83. data2 = fscanf(fin2,'%g %g',[2 inf]);
84. fclose(fin2);
85. tempsim = data2(2,:);
86. timesim = data2(1,:);
87. %%%%%%%%%%%%%%%%%%%%%%%%%%%%%%%%%%%%%%%%%%%%%%%%%%%%%%%%%%
    %%%
88. %% Normalization of temperature data obtained from simulation
89. tempsimf= zeros(1, N);
90. for i=1:N+1
91.     tempsimf(i)= (tempsim(i)-min(tempsim))/(max(tempsim)-min(tempsim));
92. end
93. model.hist.disable;
94. %%%%%%%%%%%%%%%%%%%%%%%%%%%%%%%%%%%%%%%%%%%%%%%%%%%%%%%%%%
    %%%
95. %% Error calculation between experiment and simulation data at each time
    interval
96. %which is to be minimized
97. error=0;          % initialization of error
98. for i=1:N
99.     error = error + (tempsimf(i) - TempX(i))^2;
100.     end
101.     %%%%%%%%%%%%%%%%%%%%%%%%%%%%%%%%%%%%%%%%%%%%%%%%%%%%%%%%%%
        %%%Plotting the normalized experiment and simulation data
102.     hold on;
103.     figure(1);
104.     h=plot(TimeX,TempX,'r.-');
105.     hold on
106.     Simulated_data = plot(timesim,tempsimf,'b-');

```

```

107.         legend(h,'Experiment','Simulation', 'Location','SE')
108.         title( 'Fitting of Experiment vs Simulation Data ')
109.         xlabel('Time, s')
110.         ylabel('Normalized Temperature')
111.     grid on
112.     %%%%%%%%%%% Showing the values in MATLAB during program
        running to find optimized value
113.     OptX = [cond_fluid; r_int; 1e6*p_laser];
114.     %% Saving the control parameters and error values in text files for each
        iteration until
115.     %the final optimized parameters are determined.
116.     fout=fopen('position_rs.txt','a+');
117.         fprintf(fout,'%6.4e %g %6.4e\n',OptX);
118.         fclose('all');
119.     f1=error;
120.     fout=fopen('error_rs.txt','a+');
121.         fprintf(fout,'%g\n',f1);
122.         fclose('all');
123.     %% Display the control parameters and error values during the
        optimization process
124.     k_r_q = OptX'
125.     error
126.     end
%%%%%%%%%%END of program %%%%%%%%%%%

```

## REFERENCES

1. Bojin, Florina, Andreea Robu, Maria I. Bejenariu, Valentin Ordodi, Emilian Olteanu, Ada Cean, Roxana Popescu, Monica Neagu, Oana Gavriiliuc, Adrian Neagu, Stelian Arjoca, and Virgil Păunescu. 2021. "3D Bioprinting of Model Tissues That Mimic the Tumor Microenvironment" *Micromachines* 12, no. 5: 535. <https://doi.org/10.3390/mi12050535>
2. McGarry, C. K., Grattan, L. J., Ivory, A. M., Leek, F., Liney, G. P., Liu, Y., ... & Clark, C. H. (2020). Tissue mimicking materials for imaging and therapy phantoms: a review. *Physics in Medicine & Biology*, 65(23), 23TR01.
3. Weiswald, L. B., Bellet, D., & Dangles-Marie, V. (2015). Spherical cancer models in tumor biology. *Neoplasia (New York, N.Y.)*, 17(1), 1–15. <https://doi.org/10.1016/j.neo.2014.12.004>
4. H. Samadian, S. Jafari, M.R. Sepand, L. Alaei, S. Sadegh Malvajerd, M. Jaymand, F. Ghobadinezhad, F. Jahanshahi, M.R. Hamblin, H. Derakhshankhah, Z. Izadi, 3D bioprinting technology to mimic the tumor microenvironment: tumor-on-a-chip concept, *Materials Today Advances*, Volume 12, 2021, 100160, ISSN 2590-0498, <https://doi.org/10.1016/j.mtadv.2021.100160>.
5. Kan Wang, Chia-Che Ho, Chuck Zhang, Ben Wang, A Review on the 3D Printing of Functional Structures for Medical Phantoms and Regenerated Tissue and Organ Applications, *Engineering*, Volume 3, Issue 5, 2017, ages 653-662, ISSN 2095-8099, <https://doi.org/10.1016/J.ENG.2017.05.013>.
6. Hoarau-Vechot J, Rafii A, Touboul C, Pasquier J. Halfway between 2D and Animal Models: Are 3D Cultures the Ideal Tool to Study Cancer-Microenvironment Interactions? *International journal of molecular sciences*. 2018;19(1). Epub 2018/01/19. doi: 10.3390/ijms19010181. PubMed PMID: 29346265; PMCID: PMC5796130.
7. Caragher S, Chalmers AJ, Gomez-Roman N. Glioblastoma's Next Top Model: Novel Culture Systems for Brain Cancer Radiotherapy Research. *Cancers (Basel)*. 2019;11(1). Epub 2019/01/10. doi: 10.3390/cancers11010044. PubMed PMID: 30621226; PMCID: PMC6356812.
8. Tso CL, Freije WA, Day A, Chen Z, Merriman B, Perlina A, Lee Y, Dia EQ, Yoshimoto K, Mischel PS, Liau LM, Cloughesy TF, Nelson SF. Distinct transcription profiles of primary and secondary glioblastoma subgroups. *Cancer Res*. 2006;66(1):159-67. Epub 2006/01/07. doi: 10.1158/0008-5472.CAN-05-0077. PubMed PMID: 16397228.
9. Shrestha, R., Atluri, R., Simmons, D. P., Kim, D. S., & Choi, T. Y. (2018). A micro-pipette thermal sensing technique for measuring the thermal conductivity of

10. Shrestha, R., Atluri, R., Simmons, D. P., Kim, D. S., & Choi, T. Y. (2020). Thermal conductivity of a Jurkat cell measured by a transient laser point heating method. *International Journal of Heat and Mass Transfer*, 160, 120161. non-volatile fluids. *Review of Scientific Instruments*, 89(11), 114902.
11. Paul, A., Narasimhan, A., Das, S. K., Sengupta, S., & Pradeep, T. (2016). Subsurface thermal behavior of tissue mimics embedded with large blood vessels during plasmonic photo-thermal therapy. *International Journal of Hyperthermia*, 32(7), 765-777.
12. Negussie, A. H., Partanen, A., Mikhail, A. S., Xu, S., Abi-Jaoudeh, N., Maruvada, S., & Wood, B. J. (2016). Thermochromic tissue-mimicking phantom for optimization of thermal tumor ablation. *International journal of hyperthermia : the official journal of European Society for Hyperthermic Oncology, North American Hyperthermia Group*, 32(3), 239–243.  
<https://doi.org/10.3109/02656736.2016.1145745>.
13. Xie, B., Singh, R., Torti, F. M., Keblinski, P., & Torti, S. (2012). Heat localization for targeted tumor treatment with nanoscale near-infrared radiation absorbers. *Physics in Medicine & Biology*, 57(18), 5765.
14. Fuentes, D., Oden, J. T., Diller, K. R., Hazle, J. D., Elliott, A., Shetty, A., & Stafford, R. J. (2009). Computational modeling and real-time control of patient-specific laser treatment of cancer. *Annals of biomedical engineering*, 37(4), 763-782.
15. Singh, S., & Melnik, R. (2020). Thermal ablation of biological tissues in disease treatment: A review of computational models and future directions. *Electromagnetic biology and medicine*, 39(2), 49-88.
16. Sokolovskaya, O. I., Sergeeva, E. A., Golovan, L. A., Kashkarov, P. K., Khilov, A. V., Kurakina, D. A., ... & Kirillin, M. Y. (2021, December). Numerical Simulation of Enhancement of Superficial Tumor Laser Hyperthermia with Silicon Nanoparticles. In *Photonics* (Vol. 8, No. 12, p. 580). Multidisciplinary Digital Publishing Institute.
17. Soltani, M., Tehrani, M. H., Kashkooli, F. M., & Rezaeian, M. (2020). Effects of magnetic nanoparticle diffusion on microwave ablation treatment: A numerical approach. *Journal of Magnetism and Magnetic Materials*, 514, 167196.
18. Banerjee, R., Chandran, N., Paruchuri, S., & Myers, M. High-Intensity Focused Ultrasound energized nanoparticles-mediated enhanced thermal ablation of tumors: Recent Progress and a Proposed Method for Distinguishing Heat Sources. *Annual Review of Heat Transfer*.
19. Ashikbayeva, Z., Tosi, D., Balmassov, D., Schena, E., Saccomandi, P., & Inglezakis, V. (2019). Application of nanoparticles and nanomaterials in thermal ablation therapy of cancer. *Nanomaterials*, 9(9), 1195.

20. Fernandes, D. A., Fernandes, D. D., Malik, A., Gomes, G. N. W., Appak-Baskoy, S., Berndl, E., ... & Kolios, M. C. (2021). Multifunctional nanoparticles as theranostic agents for therapy and imaging of breast cancer. *Journal of Photochemistry and Photobiology B: Biology*, 218, 112110.
21. Velliou, E., Gupta, P., Ricci, C., & Danti, S. (2020). Biomaterial-based in vitro models for pancreatic cancer. In *Biomaterials for 3D Tumor Modeling* (pp. 235-249). Elsevier.
22. Shashni, B., Ariyasu, S., Takeda, R., Suzuki, T., Shiina, S., Akimoto, K., ... & Aoki, S. (2018). Size-based differentiation of cancer and normal cells by a particle size analyzer assisted by a cell-recognition PC software. *Biological and Pharmaceutical Bulletin*, 41(4), 487-503.
23. Ficorella, C., Vázquez, R. M., Heine, P., Lepera, E., Cao, J., Warnt, E., ... & Käs, J. A. (2019). Normal epithelial and triple-negative breast cancer cells show the same invasion potential in rigid spatial confinement. *New Journal of Physics*, 21(8), 083016.
24. Cellink <https://www.cellink.com/bioprinting/bio-x-3d-bioprinter/>, accessed on 21 April 2022.
25. COMSOLMultiphysics, <https://www.comsol.com/model/modeling-of-material-heating-via-the-beer-lambert-law-46701>, accessed on 21 April 2022.
26. COMSOLMultiphysics, <https://www.comsol.com/blogs/modeling-laser-material-interactions-with-the-beer-lambert-law>, accessed on 21 April 2022.
27. COMSOLMultiphysics, [https://www.comsol.com/model/download/731361/models.mph.laser\\_heating\\_wafer.pdf](https://www.comsol.com/model/download/731361/models.mph.laser_heating_wafer.pdf), accessed on 21 April 2022.